

ASSESSING THE ACCURACY OF GEOREFERENCED POINT CLOUDS FROM UAS IMAGERY

Edward R. Clay¹, Kara S. Lee¹, Sheng Tan¹, Long Ngo Hoang Truong², Omar E. Mora^{1*}, Wen Cheng¹

¹Civil Engineering Department, California State Polytechnic University, Pomona, USA – (erclay, karalee, shengtan, oemora, and wcheng)@cpp.edu

²Department of Computer Science, California State Polytechnic University, Pomona, USA – ltruong@cpp.edu

KEY WORDS: Unmanned Aircraft System (UAS), Ground Control Point (GCP), Photogrammetry, Accuracy, Root Mean Square Error (RMSE), Point Clouds.

ABSTRACT:

Unmanned Aircraft System (UAS) mapping methods determine the three-dimensional (3D) position of surface features. UAS mapping is often used, compared to traditional mapping techniques, such as the total station (TS), Global Navigation Satellite System (GNSS) and terrestrial laser scanning (TLS). Traditional mapping methods have become less favourable due to efficiency and cost, especially for medium to large areas. As UAS mapping increases in popularity, the need to verify its accuracy for topographic mapping is evident. In this study, an assessment of the accuracy of UAS mapping is performed. Our results suggest that there are many factors that affect the accuracy of UAS photogrammetry products. In specific, the distribution and density of ground control points (GCPs) are particularly significant for a study area of 2.861 km² in size. The best results were obtained by strategizing the distribution and density of GCPs; where, the root mean square error (RMSE) for the X, Y, Z, and 3D was minimized to 0.012, 0.021, 0.038, and 0.045 meters, respectively, by applying a total of 15 GCPs in the aerotriangulation. Therefore, it may be concluded that UAS photogrammetric mapping can meet sub-decimeter accuracy for topographic mapping, if proper planning, data collection and processing procedures are followed.

1. INTRODUCTION

Topographic mapping supports civil, construction, and environmental engineering applications (Lui et al., 2014). Current topographic mapping techniques include the Global Navigation Satellite System (GNSS), Light Detection and Ranging (LiDAR), and total station (Mitasova et al., 2004). However, these methods are time consuming, labor intensive, and costly. For these reasons, new techniques are needed.

In the last decade, the advancements made in topographic mapping techniques offer a unique opportunity to map and model surfaces at unprecedented scales (Kennie, 2014). In particular, the improvements made in Unmanned Aircraft Systems (UASs) coupled with vision-based systems and computer vision algorithms provide new opportunities for collecting, processing, and reconstructing the three-dimensional (3D) position of surface features (Colomina and Molina, 2014). UASs fused with vision-based systems provide unique advantages for noncontact, high temporal, and spatial resolution data (Rakha and Gorodetsky, 2018; Mora et al., 2019). The improvements made in both UASs, and vision-based systems have caused UASs to become an affordable and flexible option for topographic mapping. The eased restrictions on commercial drone use from the Federal Aviation Administration (FAA) has led to a surge in research and commercial services involving lightweight UAS (Love et al., 2015). As the advantages of UAS become clear, the adoption of UASs increases in parallel (Vincenzi et al., 2014).

Currently, many UASs equipped with vision-based systems have been developed for topographic mapping (Lu et al., 2018; Opromolla et al., 2018). Applications include stockpile estimation, 3D modeling, planimetry extraction, and topographic mapping (Sanfourche et al., 2012; Alsalam et al., 2017; Mora et al., 2020). Ongoing developments for UASs are based on photogrammetry and computer vision algorithms (Dandois and Ellis, 2013; Rakha et al., 2018). Other studies focus on the impact of flying height, overlap, environmental conditions and optical sensor models (Seifert et al., 2019). Although the results from prior studies are promising, a study focused on the performance

of a UAS coupled with a vision-based system for medium to large areas is not well understood.

In this study, the results of an experimental evaluation to assess the accuracy of UAS photogrammetry for topographic mapping for medium to large areas is performed. Imagery is collected by using a Phantom 4 Pro v2.0 over a test site having 25 Ground Control Points (GCPs) covering an area of 2.861 km². Subsequently, the imagery is processed using Bentley ContextCapture. Then, the accuracy is evaluated by using the checkpoints to compute the root mean square error (RMSE) for the X, Y, Z, and 3D. The results observed demonstrated that RMSE values up to 0.012, 0.021, 0.038, and 0.045 meters for the X, Y, Z, and 3D, respectively, can be achieved when a total of 15 GCPs are applied in the aerotriangulation. Therefore, it may be concluded that UAS photogrammetric mapping can meet sub-decimeter accuracy for topographic mapping, if proper planning, data collection and processing procedures are followed.

2. MATERIALS AND METHODS

The procedure used to evaluate the photogrammetric mapping accuracy of UAS surveys is summarized in Figure 1.

2.1 Study Area

The study area is in Spadra Farm (Pomona), Southern California, United States of America (Latitude: 34° 02' 21.73" N, Longitude: 117° 48' 59.44" W). The study site has an area of 2.861 km². The selection of the study site was based on its morphology, which is primarily an agricultural field. The elevation range is 47.78 meters, varying from 189.60 to 237.38 meters in the North American Vertical Datum of 1988. The study area has some vegetation from the crops in the agriculture field as shown in Figure 2.

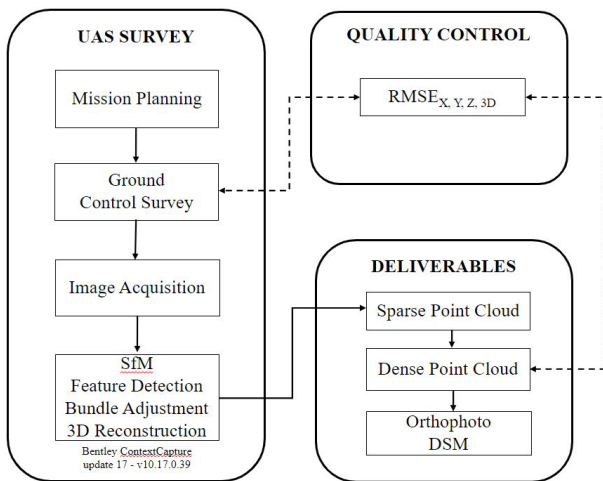


Figure 1. Flowchart of the methodology.

2.2 Image Acquisition

The images were acquired from a Phantom 4 Pro v2.0. The UAS was equipped with a camera sensor of 20 megapixels ($5,472 \times 3,648$) and a mechanical shutter. The flight altitude was 120 meters above ground level, which implies an equivalent ground sample distance of 34.2 mm/pixel. The shutter speed was adjusted based on flight altitude, UAS speed, and lighting conditions at flight time to minimize image blurring. The mission was carried out autonomously using the software DroneDeploy, where a total of 13 flight lines and 1,051 images were acquired. The flight was set to obtain a forward and side overlap of 80 and 70 %, respectively.

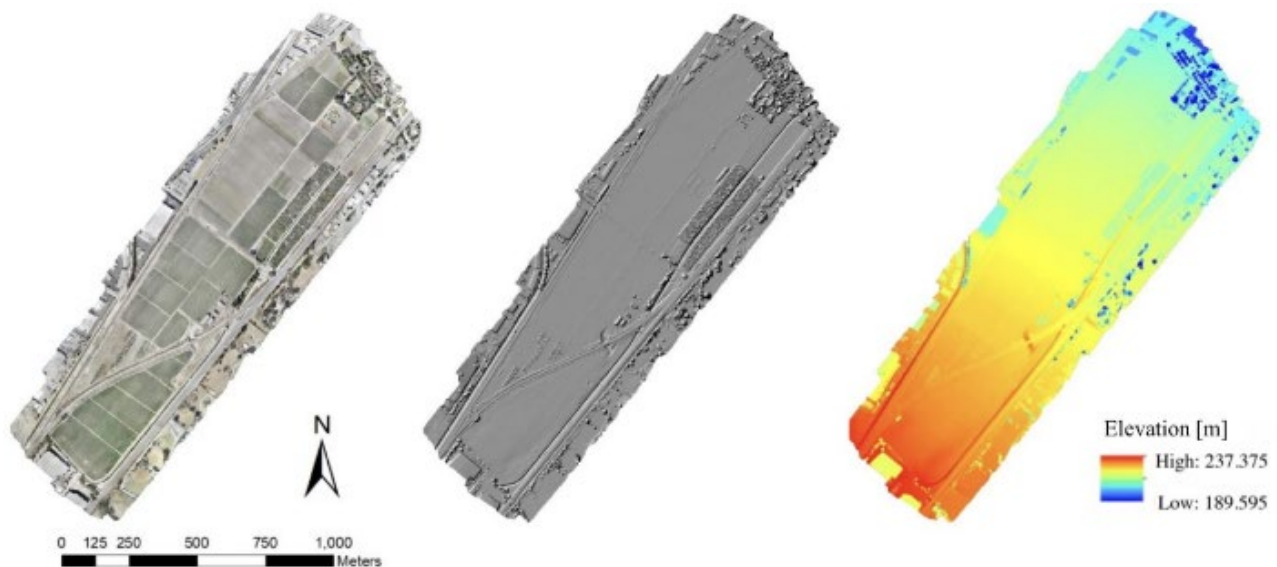


Figure 2. Study area location within the city limits of Pomona in Los Angeles County, California, USA.

2.5 Accuracy Assessment

The accuracy of all photogrammetric projects was evaluated using the checkpoints that were not used for georeferencing, using the root mean square error (RMSE) formulation. To this end, the checkpoints were identified in the point clouds, and their corresponding surveyed GNSS coordinates were compared, resulting in $RMSE_X$, $RMSE_Y$, $RMSE_Z$, and $RMSE_{3D}$, as defined in equations 1 – 4 (Chai & Draxler, 2014).

2.3 Ground Control Points

Before the image acquisition took place, 25 GCPs were set around the project site to assess the UAS survey's accuracy. Some of the GCPs will be used as checkpoints, while the others will be used as GCPs in the aertotriangulation. The three-dimensional coordinates of the GCPs were measured with a GNSS rover in Real-Time Kinematic (RTK) mode, with the base station located within the project site. The horizontal coordinates were processed to the California State Plane Coordinate System Zone 5, while the vertical was in the North American Vertical Datum of 1988. Both base and rover systems were Trimble R10 systems. Given that the base was within the project site, both the horizontal and vertical errors were ± 2 cm.

2.4 Photogrammetric Processing

The photogrammetric process was carried out using Bentley ContextCapture, update 17 - v10.17.0.39. This photogrammetric software is based on the structure-from-motion methodology. The workflow follows a four-step process. The first step is to import the imagery and GCPs/checkpoints. The second step is to perform the photo ID to identify all GCPs/checkpoints in all corresponding images. The third step is to align the images by automatic feature identification and matching. The software simultaneously estimates both the internal and external parameters, including radial and tangential distortion. The result of this step is the camera position corresponding to each image, the internal camera calibration parameters, and the 3D coordinates of a sparse point cloud of the terrain. The final step is to apply texture to the mesh. In general, the bundle adjustment can be carried out using a minimum of three GCPs; however, better results are obtained using more GCPs, which is recommended to achieve the best accuracy.

$$RMSE_X = \sqrt{\frac{\sum_{i=1}^n (X_i - X_{GNSS_i})^2}{n}}, \quad (1)$$

$$RMSE_Y = \sqrt{\frac{\sum_{i=1}^n (Y_i - Y_{GNSS_i})^2}{n}}, \quad (2)$$

$$RMSE_Z = \sqrt{\frac{\sum_{i=1}^n (Z_i - Z_{GNSS_i})^2}{n}}, \quad (3)$$

$$RMSE_{3D} = \sqrt{\frac{\sum_{i=1}^n (3D_i - 3D_{GNSS_i})^2}{n}}, \quad (4)$$

where, n = number of checkpoints tested for each project
 X_i, Y_i, Z_i , and $3D_i$ = coordinates estimated from the bundle adjustment for the i^{th} checkpoint.
 $X_{GNSS}, Y_{GNSS}, Z_{GNSS}$, and $3D_{GNSS}$ = coordinates measured with GNSS for the i^{th} checkpoint.

2.6 Experimental Tests

To evaluate the impact of the density and distribution of the GCPs, twelve different tests were performed in the photogrammetric bundle adjustment. The twelve tests were evaluated with varying GCPs ranging from 4 – 15 and checkpoints ranging from 10 – 21. The location of the GCPs and checkpoints used in the experimental tests are shown in Figure 3.

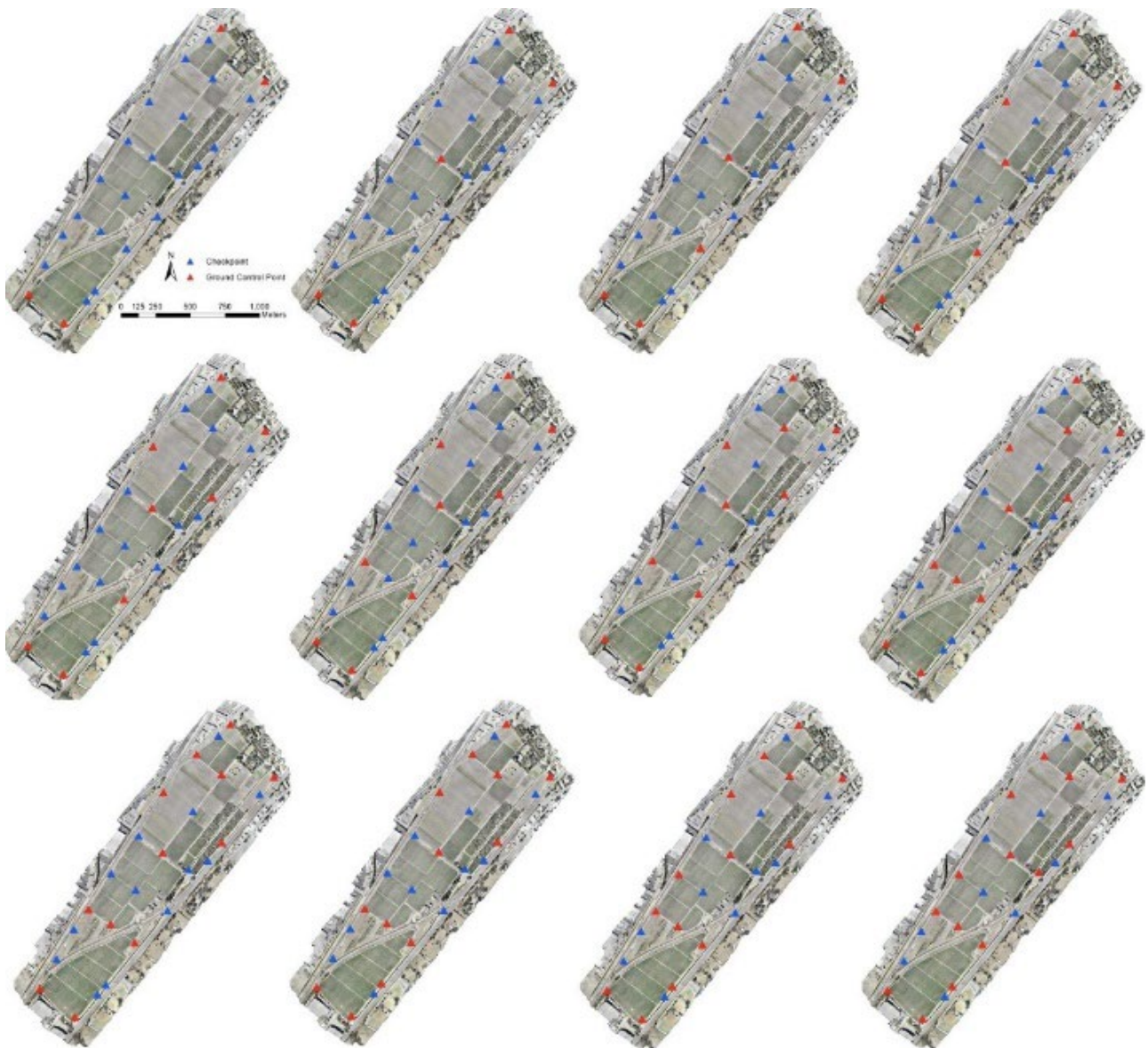


Figure 3. Twelve experimental tests were evaluated with varying distribution of GCPs and checkpoints.

3. RESULTS

The results are summarized in Table 1 and Figure 4 for all twelve tests. As a general remark the accuracy is significantly influenced by the number of GCPs applied in the aerotriangulation, especially for a test site of 2.861 km² in size. Although one would expect the accuracy performance to increase gradually by increasing the number of GCPs, an optimal performance level will be reached. At its best performance, the RMSE values will not improve significantly by adding additional GCPs in the aerotriangulation. On the contrary, the additional effort needed to add an additional GCP to the aerotriangulation may outweigh

the benefits of the additional GCP (e.g., planning, data collection, and processing). For these reasons, it is critical to know the desired accuracy needed prior to project planning to determine the optimal number of GCPs needed to achieve this goal. As shown in Table 1 and Figure 4, the overall error decreases as the number of applied GCPs increases. This supports the notion that higher levels of accuracy can be reached by using more GCPs, as suggested by earlier studies (Martínez-Carricondo et al., 2018; Sanz-Ablanedo et al., 2018). There is a notable exception to this observed in our testing. The implementation of 9 GCPs produces lower RMSE values than 10, 11 or 12 GCPs in the aerotriangulation. One potential justification for this could be

the visual quality of the GCPs in question (Montazeri, S. et al., 2018). The issue of visibility does not necessarily mean that a physical obstruction prevents accurate readings of the GCP but could also include light level, humidity, and air quality (Bałazy et al., 2019). Another potential explanation revolves around the distribution of the GCPs being used in higher concentrations in a particular area (James, M. R. et al., 2017; Guntel, A. et al., 2018). Shown in Table 1 and Figure 4 is a large RMSE_Z value of 4.721 m when applying four GCPs in the aerotriangulation. This issue is evident for an area 2.861 km² in size, where the bundle adjustment may not be able to properly solve for the camera

calibration parameters (Zheng et al., 2015). Preferably, the camera calibration parameters should be approximated in a laboratory environment, however, these parameters often change from flight-to-flight (Zhou et al., 2020; Lim et al., 2019). Another issue with only applying four GCPs may be due to the density and distribution of the GCPs, where there is no single GCP available to support the bundle adjustment for a span of about 1.610 km. This issue can be resolved by adding an additional GCP in the middle of the study area as shown in Figure 3. The RMSE_Z value is significantly improved by 4.615 m to 0.106 m.

Accuracy Results

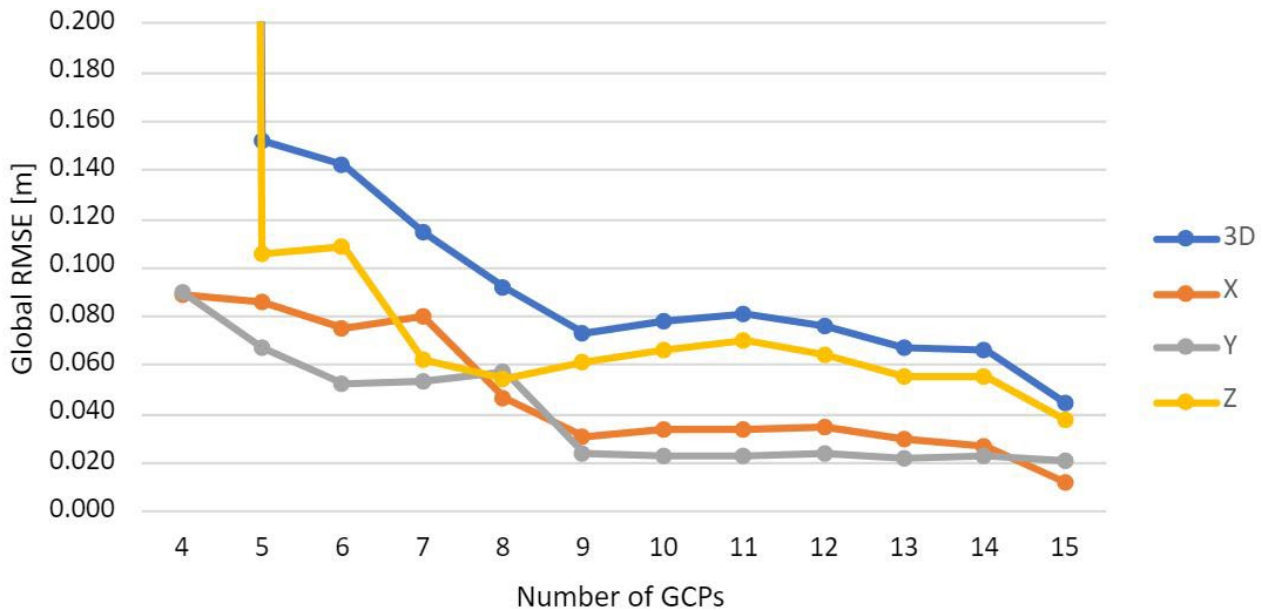


Figure 4. Summary of Accuracy Results

No. of GCPs	Reprojection Error [pixels]	Distances to Rays [m]	3D Error [m]	RMSE _X [m]	RMSE _Y [m]	RMSE _Z [m]
4	67.170	1.939	4.723	0.089	0.090	4.721
5	3.300	0.110	0.152	0.086	0.068	0.106
6	3.010	0.098	0.142	0.075	0.053	0.109
7	2.890	0.096	0.115	0.080	0.054	0.062
8	2.340	0.078	0.092	0.047	0.057	0.054
9	1.550	0.051	0.073	0.031	0.024	0.062
10	1.620	0.053	0.078	0.034	0.023	0.066
11	1.620	0.053	0.081	0.034	0.023	0.070
12	1.590	0.053	0.077	0.035	0.024	0.064
13	1.500	0.050	0.067	0.030	0.022	0.056
14	1.490	0.049	0.066	0.027	0.023	0.055
15	1.290	0.043	0.045	0.012	0.021	0.038
Mean	7.448	0.223	0.476	0.048	0.040	0.455
Median	1.620	0.053	0.080	0.035	0.024	0.063
Min	1.290	0.043	0.045	0.012	0.021	0.038
Max	67.170	1.939	4.723	0.089	0.090	4.721

Table 1. Summary of Global RMSE Results

This study provides an independent evaluation of the performance of the bundle adjustment since a different number of GCPs and checkpoints were tested. The GCPs were distributed throughout the study area as shown in Figure 3. The density and distribution of the GCPs for a site with agricultural morphology is critical to improve the performance of the bundle adjustment

and to minimize the RMSE values for a medium to large project area. The differences between the UAS-derived point cloud and GNSS RTK measurements were investigated. The results observed feature the quality of the accuracy of the UAS point cloud. These results are stable and provide confidence that a

quality high-resolution point cloud from UAS photogrammetric surveys is possible when proper procedures are followed.

4. CONCLUSIONS

As a result of the above analysis, it is essential to prepare a comprehensive study of the number of the GCPs to exploit the accuracy of photogrammetric projects. To obtain the best RMSE in X, Y, Z, and 3D, the distribution and density of the GCPs must be placed strategically. As the project size increases, the number of GCPs will increase until the desired RMSE accuracy results are achieved. When planning a UAS photogrammetric survey, sufficient GCPs must be distributed and placed strategically throughout the project site. However, this may be a challenge due to access to a site or dangerous site conditions. For these reasons, it is critical that during planning, the anticipated RMSE is well understood given the density and distribution of the GCPs. In this study, the best results were obtained by minimizing the RMSE for the X, Y, Z, and 3D to 0.012, 0.021, 0.038, and 0.045 meters, respectively, by applying a total of 15 GCPs in the aerotriangulation. Therefore, the results support that UAS photogrammetric surveys can meet sub-decimeter accuracy for topographic mapping, if proper planning, data collection and processing procedures are followed.

ACKNOWLEDGEMENTS

The authors want to thank the WestLAND Group, Inc. for helping with the data collection for this study.

REFERENCES

- Guntel, A., Karabork, H., & Karasaka, L. (2018). Accuracy Analysis of Control Point Distribution for Different Terrain Types on Photogrammetric Block. *Tehnički vjesnik*, 25(Supplement 1), 66-74.
- James, M. R., Robson, S., d'Oleire-Oltmanns, S., & Niethammer, U. (2017). Optimising UAV topographic surveys processed with structure-from-motion: Ground control quality, quantity and bundle adjustment. *Geomorphology*, 280, 51-66.
- Map Scales, Fact Sheet FS105-02, (February 2002)
- Montazeri, S., Gisinger, C., Eineder, M., & Xiang Zhu, X. (2018). Automatic detection and positioning of ground control points using TerraSAR-X multiaspect acquisitions. *IEEE Transactions on Geoscience and Remote Sensing*, 56(5), 2613-2632.
- Sanz-Ablanedo, E., Chandler, J. H., Rodríguez-Pérez, J. R., & Ordóñez, C. (2018). Accuracy of unmanned aerial vehicle (UAV) and SfM photogrammetry survey as a function of the number and location of ground control points used. *Remote Sensing*, 10(10), 1606.
- Ali, T. A. (2012). Positioning with Wide-Area GNSS Networks: Concept and Application. *Positioning*, 3, 1-6.
- Alsalam, B. H. Y., Morton, K., Campbell, D., & Gonzalez, F. (2017, March). Autonomous UAV with vision based on-board decision making for remote sensing and precision agriculture. In 2017 IEEE Aerospace Conference (pp. 1-12). IEEE.
- ASPRS. (2014). ASPRS Accuracy Standards for Digital Geospatial Data. In American Society of Photogrammetry and Remote Sensing.
- Bałaży, R., Kamińska, A., Ciesielski, M., Socha, J., & Pierzchalski, M. (2019). Modeling the effect of environmental and topographic variables affecting the height increment of Norway spruce stands in mountainous conditions with the use of LiDAR data. *Remote Sensing*, 11(20), 2407.
- Carson, W. W., & Reutebuch, S. E. (1997). A rigorous test of the accuracy of USGS digital elevation models in forested areas of Oregon and Washington. In *Volume 1 surveying and cartography: 1997 ACSM/ASPRS Annual convention and exposition technical paper*; Seattle, WA; April 7-10, 1997: 133-143.
- Chai, T., & Draxler, R. R. (2014). Root mean square error (RMSE) or mean absolute error (MAE)? -Arguments against avoiding RMSE in the literature. *Geoscientific model development*, 7(3), 1247-1250.
- Colomina, I., & Molina, P. (2014). Unmanned aerial systems for photogrammetry and remote sensing: A review. *ISPRS Journal of photogrammetry and remote sensing*, 92, 79-97.
- Dandois, J. P., & Ellis, E. C. (2013). High spatial resolution three-dimensional mapping of vegetation spectral dynamics using computer vision. *Remote Sensing of Environment*, 136, 259-276.
- Gesch, D. B., Oimoen, M. J., & Evans, G. A. (2014). Accuracy assessment of the US Geological Survey National Elevation Dataset, and comparison with other large-area elevation datasets: SRTM and ASTER (Vol. 1008). US Department of the Interior, US Geological Survey.
- Kennie, T. J. (2014). *Engineering surveying technology*. CRC Press.
- Lim, P. C., Seo, J., Son, J., & Kim, T. (2019). Analysis of orientation accuracy of an UAV image according to camera calibration. *Int. Arch. Photogramm. Remote Sens. Spat. Inf. Sci.*, 437-442.
- Liu, P., Chen, A. Y., Huang, Y. N., Han, J. Y., Lai, J. S., Kang, S. C., ... & Tsai, M. H. (2014). A review of rotorcraft unmanned aerial vehicle (UAV) developments and applications in civil engineering. *Smart Struct. Syst*, 13(6), 1065-1094.
- Love, C. D., Lawson, S. T., & Holton, A. E. (2015). News from above: First amendment implications of the Federal Aviation Administration ban on commercial drones. *BUJ Sci. & Tech. L.*, 21, 22.
- Lu, Y., Xue, Z., Xia, G. S., & Zhang, L. (2018). A survey on vision-based UAV navigation. *Geo-spatial information science*, 21(1), 21-32.
- Martínez-Carricondo, P., Agüera-Vega, F., Carvajal-Ramírez, F., Mesas-Carrascosa, F. J., García-Ferrer, A., & Pérez-Porras, F. J. (2018). Assessment of UAV-photogrammetric mapping accuracy based on variation of ground control points. *International journal of applied earth observation and geoinformation*, 72, 1-10.
- Mitasova, H., Drake, T. G., Bernstein, D., & Harmon, R. S. (2004). Quantifying rapid changes in coastal topography using

modern mapping techniques and geographic information system. *Environmental and Engineering Geoscience*, 10(1), 1-11.

Mora, O.E., Suleiman, A., Chen, J., Pluta, D., Okubo, M.H. and Josenhans, R., 2019. Comparing sUAS Photogrammetrically-Derived Point Clouds with GNSS Measurements and Terrestrial Laser Scanning for Topographic Mapping. *Drones*, 3(3), p.64.

Mora, O.E., Chen, J., Stoiber, P., Koppanyi, Z., Pluta, D., Josenhans, R. and Okubo, M., 2020. Accuracy of stockpile estimates using low-cost sUAS photogrammetry. *International Journal of Remote Sensing*, 41(12), pp.4512-4529.

Nikolov, I., & Madsen, C. (2016, October). Benchmarking close-range structure from motion 3D reconstruction software under varying capturing conditions. In *Euro-Mediterranean Conference* (pp. 15-26). Springer, Cham.

Opromolla, R., Fasano, G., & Accardo, D. (2018). A vision-based approach to UAV detection and tracking in cooperative applications. *Sensors*, 18(10), 3391.

Price, D. J. (1955). Medieval land surveying and topographical maps. *The Geographical Journal*, 121(1), 1-7.

Rakha, T., & Gorodetsky, A. (2018). Review of Unmanned Aerial System (UAS) applications in the built environment: Towards automated building inspection procedures using drones. *Automation in Construction*, 93, 252-264.

Rakha, T., Liberty, A., Gorodetsky, A., Kakillioglu, B., & Velipasalar, S. (2018). Heat mapping drones: an autonomous computer-vision-based procedure for building envelope inspection using unmanned aerial systems (UAS). *Technology| Architecture+ Design*, 2(1), 30-44.

Sanfourche, M., Delaune, J., Le Besnerais, G., De Plinval, H., Israel, J., Cornic, P., ... & Plyer, A. (2012). Perception for UAV: Vision-Based Navigation and Environment Modeling. *AerospaceLab*, (4), p-1.

Schenk, T. (2005). *Introduction to photogrammetry*. The Ohio State University, Columbus, 106.

Seifert, E., Seifert, S., Vogt, H., Drew, D., Van Aardt, J., Kunneke, A., & Seifert, T. (2019). Influence of drone altitude, image overlap, and optical sensor resolution on multi-view reconstruction of forest images. *Remote sensing*, 11(10), 1252.

Skitka, L. J., Mosier, K. L., & Burdick, M. (1999). Does automation bias decision-making?. *International Journal of Human-Computer Studies*, 51(5), 991-1006.

Uysal, M., Toprak, A. S., & Polat, N. (2015). DEM generation with UAV Photogrammetry and accuracy analysis in Sahitler hill. *Measurement*, 73, 539-543.

Vincenzi, D., Ison, D. C., & Terwilliger, B. A. (2014). *The Role of Unmanned Aircraft Systems (UAS) in Disaster Response and Recovery Efforts: Historical, Current and Future*.

Zheng, S., Wang, Z., & Huang, R. (2015). Zoom lens calibration with zoom-and focus-related intrinsic parameters applied to bundle adjustment. *ISPRS journal of photogrammetry and remote sensing*, 102, 62-72.